INSTABILITIES

K. Schindl
CERN, CH-1211 Geneva 23
E-mail: Karlheinz.Schindl@cern.ch

Abstract
What are the mechanisms leading to beam instabilities in circular accelerators? This lecture, intended for physicists and engineers with little or no knowledge on the subject, tries to answer this question. The physical concepts are presented for a few typical examples rather than attempting an exhaustive overview of the many types of coherent collective effects, impossible anyway in a one-hour lecture. As they are somewhat simpler to describe, the lecture concentrates on longitudinal instabilities.

1. BASIC MECHANISM DRIVING AN INSTABILITY

Assume a bunched beam circulating in a synchrotron. The bunches will induce electromagnetic fields in the beam pipe and give rise to image or wall currents since the beam pipe itself is a conductor. In turn, these currents generate an electromagnetic field that acts back on the beam. Under certain conditions – the discussion of which is the very aim of this lecture – the beam may become unstable.

A circulating bunch, corresponding to an a.c. beam current I_B, induces image charges on the inner surface of the vacuum chamber that circulate with the bunch (Fig. 1). Thus they form an a.c. image or wall current $-I_W$ of the same magnitude but opposite sign to the beam current.

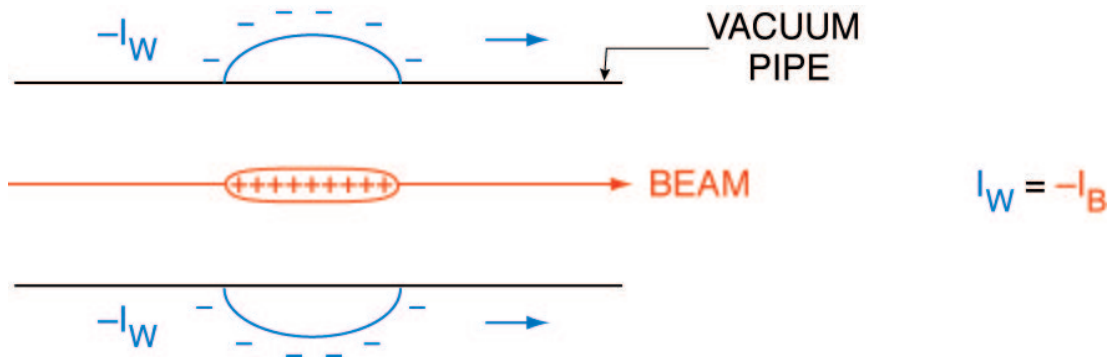

Fig. 1: Image or wall currents induced by a circulating bunch

The vacuum chamber has a finite conductivity and, moreover, changes its shape, cross-section, etc. along the beam path, and therefore presents an *impedance* to this wall current. The impedance $Z = Z_r + i\,Z_i$ can be resistive (real), capacitive or inductive (imaginary). Thus the wall current induces a voltage $V \sim I_W\,Z$ which gives rise to a longitudinal electric field, which may act back (accelerating or decelerating) on the bunch. While Z depends on the geometry and material of the vacuum enclosure and on the exciting frequency, V is proportional to the wall current and thus the beam current: *Instabilities are intensity dependent,* and in general stronger at higher beam currents.

Instabilities are investigated with the following scheme:

Step 1: Start with a nominal, unperturbed particle distribution (i.e. longitudinal position, energy, density, etc.).

Step 2: Apply a small perturbation which has a simple form – called 'mode' by the experts – and determine forces acting back on the beam.

Step 3: Calculate how the pattern would change under the forces. If it disappears, the beam is stable; if it is self-sustaining or even increases, the beam is unstable.

2. NEGATIVE MASS INSTABILITY

2.1. Qualitative treatment

This instability is no longer a problem but can be used as a starting point to understand collective effects and how they grow. Consider an unbunched beam circulating in a synchrotron. Consider furthermore a perturbation of the line density $\lambda(s)$ which describes a very simple azimuthal modulation pattern, namely eight humps around the ring (Fig. 2). Will the humps increase or erode?

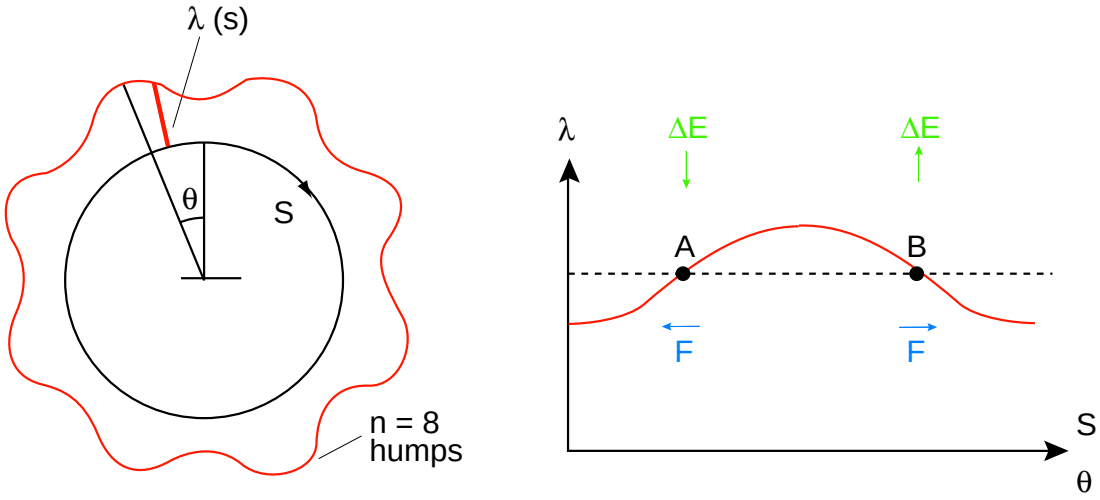

Fig. 2: Azimuthal line density modulation (left); zooming in one modulation (right)

Particle B in Fig. 2 has a larger charge density behind it, pushing it forward. Conversely, particle A will be slowed down by the hump of charge in front of it. Thus the self-force F (which is proportional to $-d\lambda/ds$) increases the energy of particle B, and decreases the energy of particle A. The stability of this 'mode' now depends on the transition gamma γ_t:

Below transition energy ($\gamma < \gamma_t$): an *increase* in energy leads to an *increase* in revolution frequency ω_0, so A and B are moving away from the hump which is eroding.

Above transition energy ($\gamma > \gamma_t$): when the energy *increases*, the revolution frequency *decreases*, so A and B move towards the summit enhancing the mountain.

So far, not a single formula was used. However, in what follows, the 'negative mass' instability is treated by a more quantitative and rigorous method, which is a complementary way to illustrate some of the concepts used in analysing instabilities.

2.2. Fields generated by the beam

An unbunched beam with modulated line density $\lambda(s)$ travels through a vacuum pipe as depicted in Fig. 3.

What is the longitudinal electrical field E_s generated by the beam? This may be evaluated by applying Stokes' law along the rectangular path in Fig. 3. The radial electrical field E_r and the azimuthal magnetic field B_ϕ are evaluated in Eq. (1), featuring the well-known linear increase proportional to radius r inside the beam, and being proportional to $1/r$ outside the beam.

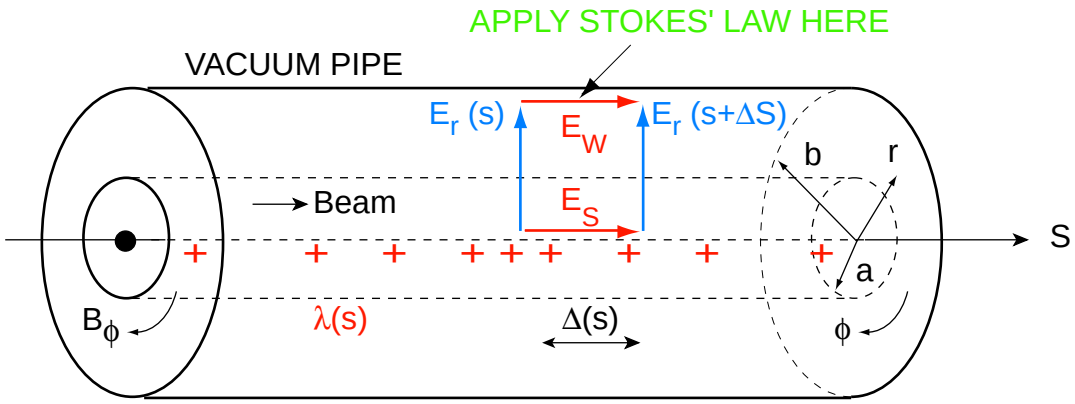

Fig. 3: Electrical (E) and magnetic (B) fields induced into a vacuum pipe (radius b) by a beam (radius a) with longitudinal density modulation $\lambda(s)$

$$\begin{aligned} E_r &= \frac{e\lambda}{2\pi\varepsilon_0}\,\frac{1}{r} \qquad B_\phi = \frac{\mu_0 e\lambda\beta c}{2\pi}\,\frac{1}{r} \qquad r \geq a\,, \\ E_r &= \frac{e\lambda}{2\pi\varepsilon_0}\,\frac{r}{a^2} \qquad B_\phi = \frac{\mu_0 e\lambda\beta c}{2\pi}\,\frac{r}{a^2} \qquad r \leq a\,. \end{aligned} \tag{1}$$

Applying Stokes' law which relates a line integral to an integral over the surface enclosed by the line

$$\oint\limits_{LINE} \vec{E}d\vec{\ell} = -\frac{\partial}{\partial t}\int\limits_{SURFACE} \vec{B}d\vec{\sigma} = -\frac{\partial}{\partial t}\,\Delta s\int\limits_0^b B_\phi\, dr \tag{2}$$

and using

$$\frac{\partial\lambda}{\partial t} = \frac{\partial\lambda}{\partial s}\,\frac{ds}{dt} = \beta c\,\frac{\partial\lambda}{\partial s} \tag{3}$$

and

$$g_0 = 1 + 2\,\ln\frac{b}{a}\,,$$

one gets for the longitudinal electrical field E_s on the beam axis

$$E_s = -\frac{eg_0}{4\pi\varepsilon_0}\,(1-\beta^2)\,\frac{\partial\lambda}{\partial s} + E_w = -\frac{eg_0}{4\pi\varepsilon_0}\,\frac{1}{\gamma^2}\,\frac{\partial\lambda}{\partial s} + E_w\,, \tag{4}$$

where E_w is the electrical field parallel to the vacuum pipe surface.

For a *perfectly conducting* wall, E_w vanishes, and one is left with

$$E_s = -\frac{eg_0}{4\pi\varepsilon_0}\,\frac{1}{\gamma^2}\,\frac{\partial\lambda}{\partial s}\,, \tag{5}$$

the *longitudinal space-charge field*, featuring the $1/\gamma^2$ dependence typical for space charge (decreasing strongly at higher energies). This is the electrical field which was used in the qualitative treatment (Section 2.1)

However, the vacuum chamber generally has a finite resistance and, in particular, an inductance due to cross-section changes, small cavity-like structures, and the like. One may lump these in an inductance per unit length $L/2\pi R$ (R radius of the synchrotron) from which one calculates E_w:

$$E_w = -\frac{L}{2\pi R}\,\frac{dI_w}{dt} \;=\; \frac{L}{2\pi R}\,e\beta c\,\frac{\partial\lambda}{\partial t} \;=\; \frac{L}{2\pi R}e\beta^2c^2\,\frac{\partial\lambda}{\partial s} \tag{6}$$

and the voltage per turn U_s along the beam path due to the inductive wall

$$U_s \;=\; e\beta cR\omega_0 L\frac{\partial\lambda}{\partial s}\,. \tag{7}$$

2.3. Fields acting back on the beam

The beam line density $\lambda(\theta)$ (with the machine azimuth $\theta \;=\; s/R$) and the corresponding instantaneous current $I(\theta)$ are basically d.c. (λ_0, I_0) with a small a.c. component of amplitude λ_1, I_1, as given below:

$$\begin{array}{ll} \lambda = \lambda_0 + \lambda_1 e^{i(n\Theta-\Omega t)} & \text{instantaneous density} \\ I = I_0 + I_1 e^{i(n\Theta-\Omega t)} & \text{instantaneous current} \end{array} \tag{8}$$

$\lambda(\theta)$ features n humps (n = 8 in the previous example). An antenna in the wall at azimuthal position θ would pick up the pattern rotating with angular frequency Ω = $n\omega_0$, and it would stay like that for a low-intensity beam. However, a non-vanishing a.c. component induces a voltage per turn of

$$\begin{array}{ccccc} U_S & = & -I_1 e^{i(n\Theta-\Omega t)} & & Z(\Omega) \\ \Downarrow & & \Downarrow & & \Downarrow \\ \text{voltage per turn} & & \text{(small) a.c. component} & & \text{longitudinal impedance} \end{array} \tag{9}$$

due to the longitudinal impedance Z which in general depends on Ω.

The trick to computing the effect of the fields acting back on the beam is to postulate that this leads to a (small) *complex frequency shift* $\Delta\Omega$ which modifies the motion of the pattern:

$$\begin{array}{ccccc} \Omega & = & n\omega_0 & + & \Delta\Omega\,. \\ \Uparrow & & \Uparrow & & \Uparrow \\ \text{perturbed frequency} & & \text{unperturbed} & & \text{(complex) frequency shift} \end{array} \tag{10}$$

While this idea appears simple, the rigorous treatment is rather involved. Instead, it is better to follow a shortcut using the well-known analysis of the motion of a particle in the longitudinal phase plane due to an external accelerating RF voltage with amplitude V_0 and frequency hf_0. The phase ϕ of a particle with respect to the RF wave satisfies the differential equation for synchrotron oscillations

$$\frac{d}{dt}\left[\frac{E_0\beta^2\gamma\dot{\phi}}{2\pi\eta hf_0^2e}\right] + V_0\,(\sin\phi - \sin\phi_s) = 0\,, \tag{11}$$

where $\eta = 1/\gamma^2 - 1/\gamma_t^2$ is the slip factor, E_0 the particle rest energy, h the RF harmonic number, and $f_0 = \omega_0/2\pi$ the revolution frequency around the synchrotron. Assuming a stable phase angle of ϕ_s = 0 (stationary bucket), small-amplitude phase oscillations (sin $\phi \approx \phi$), and neglecting the slow variation of β, γ, this equation becomes linear and features constant coefficients:

$$\left[\frac{E_0\beta^2\gamma}{2\pi\eta hf_0^2e}\right]\ddot{\phi} + V_0\phi \;=\; 0\,. \tag{12}$$

The small-amplitude synchrotron oscillation frequency is then

$$\omega_s^2 = \left[\frac{e\eta h V_0 \omega_0^2}{2\pi E_0 \beta^2 \gamma}\right] . \tag{13}$$

Here one takes an imaginative leap by replacing in Eq. (13) the term $V_0 h$ (external voltage $\times$ harmonic number) by the beam-induced voltage

$$\begin{array}{cccc} i & n & Z & I_0 \\ \Downarrow & \Downarrow & \Downarrow & \\ \text{difference in} & \text{harmonic} & \text{complex impedance} & \\ \text{phase definition} & \text{pattern} & Z = Z_r + iZ_i & \end{array}$$

yielding a frequency shift of

$$(\Delta\Omega)^2 = (\Omega - n\omega_0)^2 = -i\frac{e\eta\omega_0^2 n\, I_0}{2\pi\beta^2 E_0 \gamma}\,(Z_r + iZ_i)\,, \tag{14}$$

which happens to be the correct result! This is the (complex) frequency shift required to sustain a 'self-consistent' density modulation.

With the definition of the instantaneous current as given in Eq. (8)

$$\begin{array}{c} I(t,\Theta) = I_0 + I_1 e^{i(n\Theta - \Omega t)} = I_0 + I_1 e^{i(n\Theta - (n\omega_0 + \Delta\Omega)t)}\,, \\ \qquad\qquad\qquad\qquad\qquad\qquad\qquad\qquad \downarrow \\ \qquad\qquad\qquad\qquad\qquad\qquad\qquad\qquad \Delta\Omega_r + i\Delta\Omega_i \end{array} \tag{15}$$

where Ω is replaced by the slightly modified value $n\omega_0 + \Delta\Omega$, one gets

$$\begin{array}{c} I(t,\Theta) = I_0 + I_1 \underbrace{e^{\Delta\Omega_i t}}\, e^{i(n\Theta - (n\omega_0 + \underbrace{\Delta\Omega_r}) t)} \\ \qquad\qquad\qquad\quad \downarrow \qquad\qquad\quad \downarrow \\ \left.\begin{array}{l}\text{growth or} \\ \text{damping}\end{array}\right\} \text{of modulation pattern} \quad \text{real frequency shift}\,, \end{array} \tag{16}$$

where $\Delta\Omega_r$ is the real frequency shift of the rotating pattern, and $\Delta\Omega_i$ describes the growth or damping of the mode.

Some lengthy algebra based on Eqs. (6), (7) and (9), and use of the formula for the impedance of free space, $Z_0 = 1/\varepsilon_0 c = 377\ \Omega$, yield simplified expressions for the (capacitive) space-charge impedance

$$Z_i = \frac{n g_0 Z_0}{2\beta\gamma^2} \tag{17}$$

and the inductive impedance

$$Z_i = -n\omega_0 L\,. \tag{18}$$

The 'negative mass' instability is fully covered by Eq. (14): if the right-hand side is real and positive, $\Delta\Omega$ is real as well and there is just a real frequency shift of the rotating pattern which then remains stable. However, if the right-hand side is negative or complex, $\Delta\Omega$ has an imaginary part and is therefore always unstable.

In the qualitative treatment, the special case of a perfectly conducting wall (*resistive impedance* $Z_r = 0$) was considered. Table 1 below is based on Eq. (14) and shows in which situations the beam becomes unstable.

Table 1:

$Z_r = 0$	$\gamma < \gamma_t$ ($\eta > 0$)	$\gamma > \gamma_t$ ($\eta < 0$)
$Z_i > 0$ (capacitive)	$\Delta\Omega_\iota = 0 \Rightarrow$ stable	$\Delta\Omega_\iota \neq 0 \Rightarrow$ unstable
$Z_i < 0$ (inductive)	$\Delta\Omega_\iota \neq 0 \Rightarrow$ unstable	$\Delta\Omega_\iota = 0 \Rightarrow$ stable

Not surprisingly, this corresponds to the results of the qualitative treatment. A historical note: the term *'negative mass'* was coined by inspecting Eq. (12) where the term in front of $d^2\phi/dt^2$ becomes negative above transition energy ($\eta < 0$) drawing an analogy to the equation of an oscillating spring, $md^2x/dt^2 + k^2x = 0$, this term may be defined as 'mass'.

In a real synchrotron, the vacuum pipe always has some small resistance, so in general $Z_r > 0$. Then, from Eq. (13), $\Delta\Omega$ features two solutions, with one of them featuring a non-vanishing positive imaginary part, and thus – at this stage of the analysis – the line density modulation will grow under all conditions.

2.4. Stability diagram

The stability diagram is a widely used tool whose significance will become obvious in Section 3. It relates the imaginary part of $\Delta\Omega$, the growth (or damping) rate, to the complex impedance Z by plotting contours of constant growth rates ($\Delta\Omega_i$ = const) in the Z_r, Z_i plane. Simplifying Eq. (14) by lumping the expression which contains all beam parameters into a single constant ξ

$$(\Delta\Omega)^2 = -i\xi(Z_i + i\,Z_r) = \xi(Z_r - i\,Z_i) = (\Delta\Omega + i\Delta\Omega_i)^2\,, \tag{19}$$

and equating real and imaginary parts

$$\begin{gathered}\Delta\Omega_r^2 - \Delta\Omega_i^2 = \xi Z_i \Rightarrow \Delta\Omega_r = \sqrt{\xi Z_i + \Delta\Omega_i^2} \\ i2\Delta\Omega_r\Delta\Omega_i = -iZ_r\xi\end{gathered} \tag{20}$$

results in parabolic contours for $\Delta\Omega_i$ = const:

$$Z_r = 2\Delta\Omega_i\sqrt{Z_i/\xi + \Delta\Omega_i^2/\xi^2}\,. \tag{21}$$

Typical contours are shown in Fig. 4. The area where there is no growth ($\Delta\Omega_i$ = 0) is infinitely small and concentrated on the Z_i – axis, that is for Z_r = 0.

In summary, at this stage of the analysis, the negative mass instability drives any unbunched beam mode unstable due to the non-vanishing resistivity of the vacuum chamber. Fortunately, this is not true in most real machines, by virtue of a curious phenomenon called Landau damping.

3. LANDAU DAMPING

3.1. Basic idea

In real machines, not all particles in the beam move with the same frequency. Staying with the longitudinal motion as in the example of the density modulation pattern rotating around the synchrotron, the natural energy spread in the beam causes a spread in revolution frequencies (albeit for $\eta \neq 0$). The

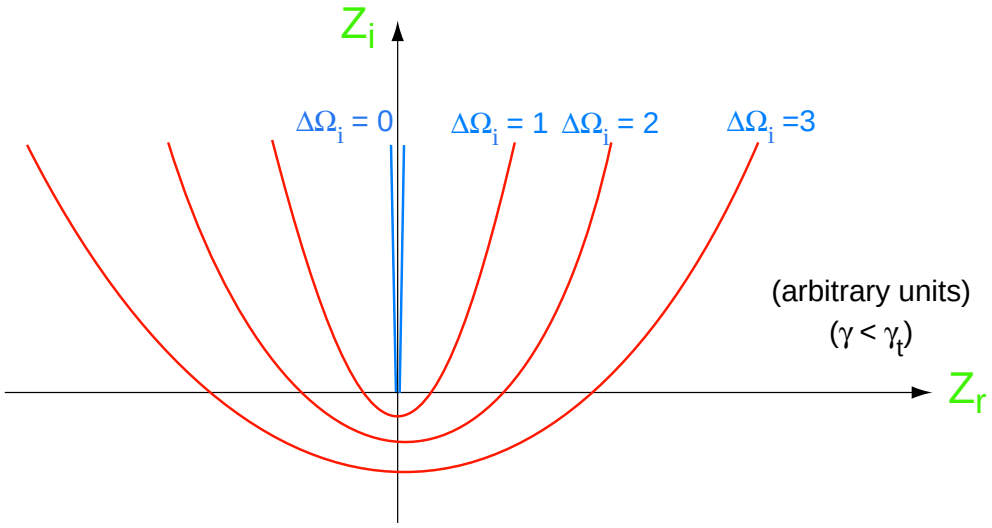

Fig. 4: Stability diagram relating growth rate $\Delta\Omega_i$ to real and imaginary part of the impedance, in arbitrary units

coherent motion imposed by the instability becomes confused and may even collapse faster than the rise time of the instability, rendering the beam stable. This is illustrated by the de-coherence of two particles, sketched in Fig. 5.

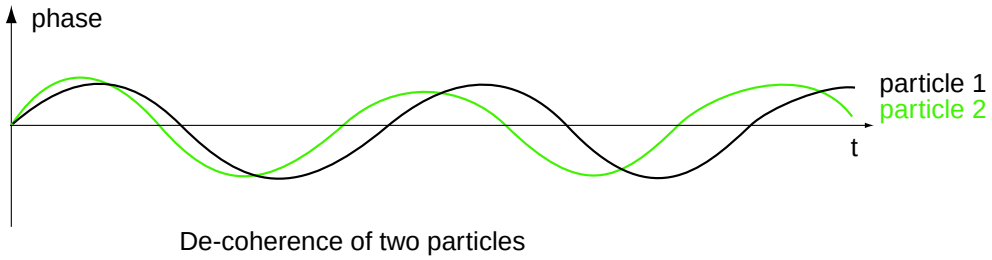

Fig. 5: De-coherence of the longitudinal motion (phase) of two particles after a longitudinal kick at $t = 0$

3.2. Landau damping – some analysis

While the basic idea appears simple, one would like to know how much of this frequency spread is actually needed to tame the instability. In what follows, an outline of the complete analysis, which is rather involved, is presented.

Consider a beam consisting of N particles, each oscillating at slightly different frequency Ω, but all of them between Ω_1 and Ω_2 with a density function g(Ω) normalized by

$$\int_{\Omega_1}^{\Omega_2} g(\Omega)\, d\Omega \;=\; 1 \tag{22}$$

and shown in Fig. 6.

How will they react on an external coherent excitation $e^{i\omega t}$ (which in fact is generated, for example, by the drive field of a longitudinal coherent instability)? The response of a single particle (with its particular resonant frequency Ω in general different from the external excitation frequency ω) is

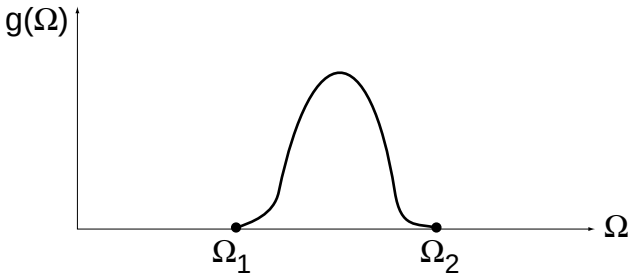

Fig. 6: Frequency density function $g(\Omega)$ for N particles oscillating at frequencies $\Omega_1 < \Omega < \Omega_2$

$$X = \frac{1}{\Omega^2 - \omega^2} e^{i\omega t} = \frac{1}{(\Omega - \omega)\underbrace{(\Omega + \omega)}_{\sim 2\Omega_0}} e^{i\omega t} \,. \tag{23}$$

To evaluate S, the overall *coherent* response to the excitation, one integrates the single-particle responses over the N oscillators

$$S = \frac{N}{2\Omega_0} \int_{\Omega_1}^{\Omega_2} \frac{i\frac{dg(\Omega)}{d\Omega}}{\Omega - \omega} d\Omega \cdot e^{i\omega t} \,. \tag{24}$$

A more thorough analysis, involving Liouville's theorem, suggests that the term $idg(\Omega)/d\Omega$, rather than $g(\Omega)$, has to be employed in Eq. (24).

If the excitation frequency ω falls outside the beam frequency range (Fig. 7a), there will be a finite coherent response S. However, things become less obvious if the excitation frequency is inside the range of the N oscillators ($\Omega_1 < \omega < \Omega_2$) (Fig. 7b), as now the integrand in Eq. (24) features a pole at $\Omega = \omega$.

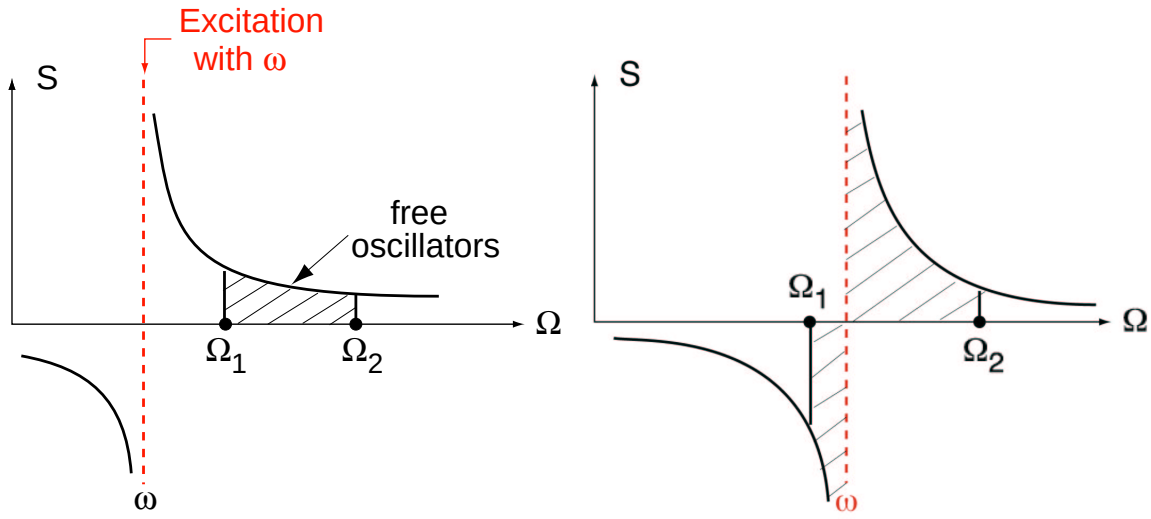

(a) (b)

Fig. 7: Coherent response S of N oscillators to an external excitation with frequency ω for (a) ω outside their frequency range (Ω_1, Ω_2), (b) ω inside the range

As described in any textbook on analysis, integral (24) can be evaluated by assuming that Ω is complex rather than real and integrating along a half-circle around the pole as depicted in Fig. 8. This procedure is not convergent in all cases, but is so in the present one.

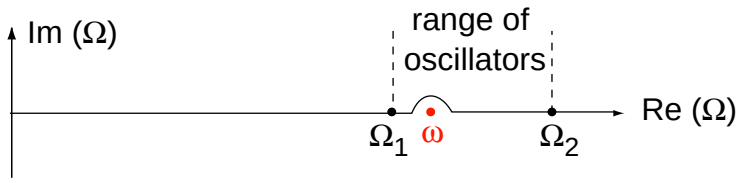

Fig. 8: Integral path in the complex Ω plane enabling the evaluation of the integral with a pole at $\Omega = \omega$ by integrating along a half-circle around the pole

Applying this recipe (Eq. 26), the integral S features a 'principal value' and a 'residuum' which can be interpreted as a 'resistive' term (absorbing energy and thus damping) and a 'reactive' term (which does not absorb energy):

$$S = i\frac{N}{2\Omega_0}\left[\int_{\Omega_1}^{\Omega_2}\frac{\frac{dg(\Omega)}{d\Omega}}{\Omega-\omega}\,d\Omega - i\Pi\right]e^{i\omega t} \quad = \quad \frac{N}{2\Omega_0}\left[-\Pi \quad + \quad i\underbrace{\int_{PV}\frac{\frac{dg(\Omega)}{d\Omega}}{\Omega-\omega}\,d\Omega}\right]e^{i\omega t}\,. \tag{25}$$

$\uparrow$ PV Principal Value; $\uparrow$ 'Residuum'; $\uparrow$ 'Resistive' term absorbs energy in phase with excitation; $\uparrow$ 'Reactive' term does not absorb energy out of phase

3.3. Stability diagram with Landau damping

The preceding analysis is the most difficult step in the evaluation of beam stability with Landau damping. Note that the amplitude A of the external excitation $Ae^{i\omega t}$ was set to 1 in the above analysis, but obviously it depends on beam current, impedance, etc. [see Eq. (14)]. Note also that there is no, or little, Landau damping whenever the beam particles are subjected to an excitation outside their frequency range; *Landau damping only works if the excitation frequency falls inside the frequency range of the beam.*

A complete analysis yields a stability diagram (Fig. 9) which dramatically differs from Fig. 4 where the beam was unstable under all conditions. Plotting the contours of equal growth rates in a Z_r, Z_i diagram (Z_r = Re(Z), Z_i = Im(Z)), one now disposes of a finite area of stability, allowing in particular for some limited resistive impedance Re(Z).

The contour with growth rate 0 is called the stability limit, inside of which the growth rate is negative (damping). The form of the stable 'bottle' depends on the distribution $g(\Omega)$, while its size scales with beam parameters like the current. For realistic ('reasonable') distribution functions, a circle can be inscribed which pretty well approximates the shape. By this technique one can derive a handy approximation for the longitudinal stability limit of unbunched beams, coined as the 'Keil–Schnell criterion':

$$\left|\frac{Z}{n}\right| \leq F\frac{m_0c^2\beta^2\gamma\,|\eta|}{e}\frac{(\Delta p/p)^2}{I_0}\,. \tag{26}$$

Here Z is the complex longitudinal impedance evaluated at $\omega = n\omega_0$, with ω_0 the average revolution frequency, m_0 the particle rest mass, $\Delta p/p$ the relative momentum spread, I_0 the beam current, and F a form factor of the order of 1, depending on the distribution.

The criterion imposes approximate threshold values for $\Delta p/p$ (minimum) and the beam intensity I_0 (maximum) beyond which, for a given impedance Z and slip factor η, the beam becomes unstable.

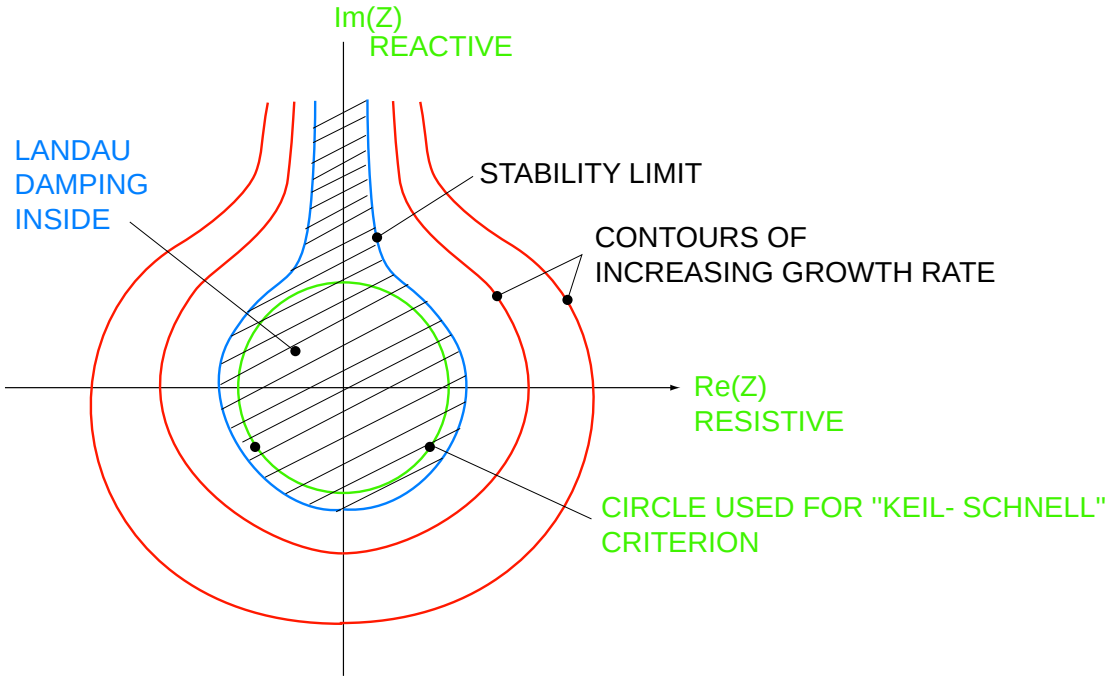

Fig. 9: Stability diagram with Landau damping, featuring a finite area of beam stability (hatched)

This longitudinal instability manifests itself in incoherent energy oscillations which are difficult to visualize; the end result is an increase in the beam's energy spread.

A final remark on Landau damping: its effect is not just limited to the negative mass instability. In fact, providing a frequency spread proves to counteract all types of beam instabilities, be they longitudinal, transverse, for unbunched or bunched beams. Thus Landau damping represents, along with active feedback systems, the most powerful tool at the disposal of accelerator physicists to tame coherent beam instabilities.

3.4. Negative mass instability – an example

This is by no means just of academic interest and may present a prohibitive performance limitation as shown in the following example. The CERN 25 GeV Proton Synchrotron (PS) is part of the LHC injector chain. Before transferring the beam to the 450 GeV SPS (the LHC injector synchrotron), short bunches (total length < 4 ns) with 25 ns spacing have to be prepared. To this end, the 16 beam bunches arriving at the PS ejection flat top are adiabatically de-bunched, and then re-bunched at $h = 84$ (25 ns spacing). The beam stays de-bunched during ~ 100 ms and is not allowed to suffer an increase in $\Delta p/p$ so as to avoid bunch lengths of more than 4 ns after re-bunching. However, this goal could initially not be achieved for the nominal LHC intensity of 8×10^{12} p as is illustrated in Fig. 10 which shows the beam frequency spread (horizontal axis) during the whole process (time goes downwards). The longitudinal machine impedance of the CERN PS is here dominated by a 114 MHz cavity (left picture) whose impedance Z at the resonance frequency is difficult to reduce (right picture). The technique used to visualize the frequency spread measures the Schottky noise. In both diagrams one starts with a large energy (frequency) spread (beam bunched on $h = 16$), which is gradually reduced by adiabatic de-bunching, until the RF is cut off and the beam is left coasting. A strong blow-up is then observed in the high-impedance case (left), which apparently does not satisfy the Keil–Schnell criterion, whereas no blow-up is observed for the lower impedance case (114 MHz cavity partially short-circuited, right).

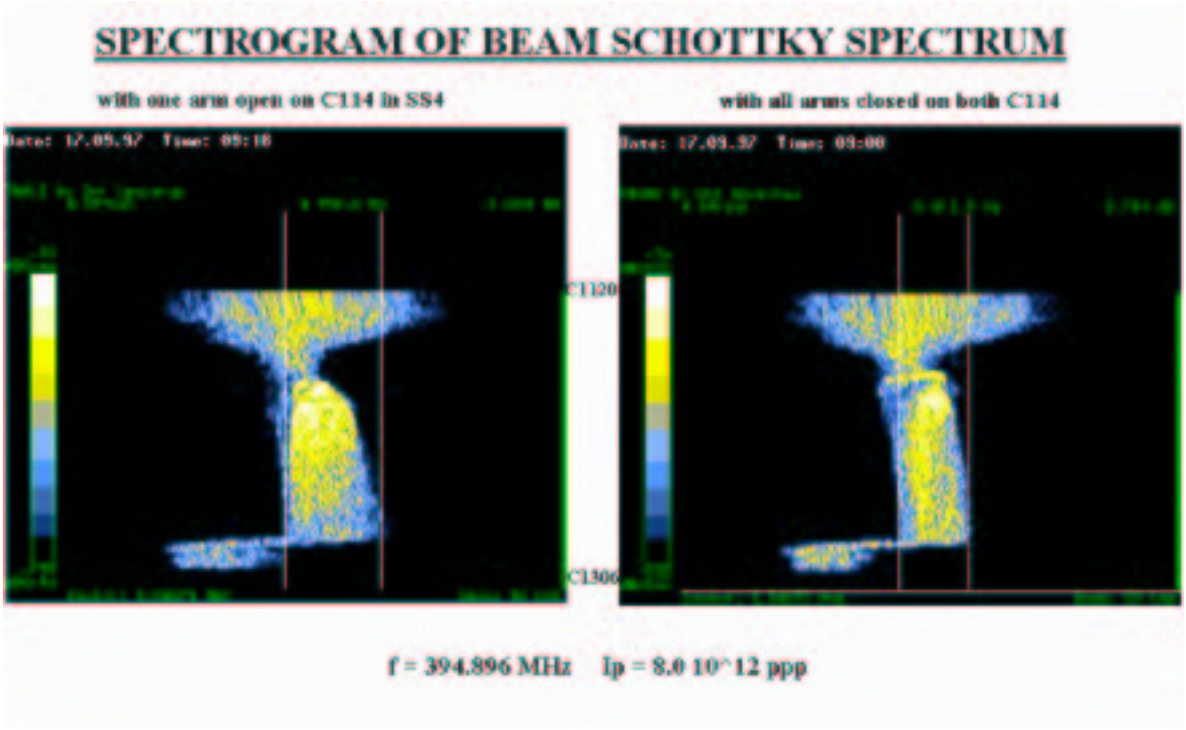

Fig. 10: Increase in momentum spread due to negative mass instability in the CERN PS during de-bunching of 8×10^{12} protons. Horizontal axis: frequency spread (proportional to momentum spread); vertical axis: time, circa 200 ms, moving downwards. Left spectrogram: high longitudinal impedance Z, beam strongly blown up. Right: low Z, now blow-up observed. See text for more details.

4. IMPEDANCE OF A RESONATOR

The machine impedance Z is a function of ω and typically takes on its largest values at the resonance frequencies of cavity-like objects which thus represent the most critical machine components, prone to drive instabilities. Therefore a closer look at these objects is worth while. The characteristic features of such objects are quite similar to a parallel RLC circuit (Fig. 11) where the a.c. current I represents the a.c. beam current, R the 'shunt impedance', ω_r the resonance angular frequency, Q the quality factor [Eq. (27)].

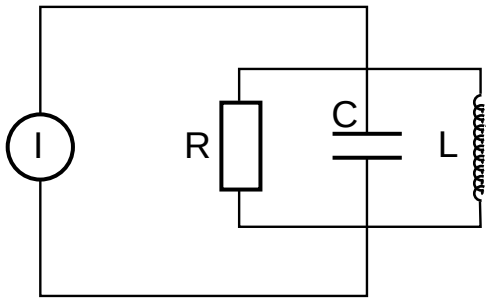

Fig. 11: Parallel RLC circuit

$$\begin{aligned} \omega_r &= \tfrac{1}{\sqrt{LC}} \quad \text{resonance frequency} \\ Q \;\; &= R\sqrt{\tfrac{C}{L}} = \tfrac{R}{\omega_r L} \quad \text{quality factor} \end{aligned} \tag{27}$$

The differential equation of the circuit is

$$\ddot{V} + \frac{\omega_r}{Q}\dot{V} + \omega_r^2 V = \omega_r \frac{R}{Q}\dot{I} \tag{28}$$

with the solution

$$V(t) = V_0\, e^{-\alpha t} \cos\left[\omega_r \sqrt{1 - 1/4Q^2}\, t + \phi\right] . \tag{29}$$

This represents a damped oscillation with the damping rate $\alpha = 1/\tau = \omega_r/2Q$.

One calculates the impedance $Z(\omega)$ by exciting the circuit with the current $I = I_0\, e^{i\omega t}$, $(-\infty < \omega < \infty)$ and looks for solutions of the form $V = V_0\, e^{i\omega t}$. Note that the range of ω includes *negative frequencies* simply because it allows doing all calculations with the more handy $e^{i\omega t}$ rather than the clumsy trigonometric functions. By virtue of Eq. 29, one then gets

$$-\omega^2 V_0\, e^{i\omega t} + i\,\frac{\omega\omega_r}{Q} V_0\, e^{i\omega t} + \omega_r^2 V_0\, e^{i\omega t} = i\,\frac{\omega_r \omega R}{Q}\, I_0\, e^{i\omega t} \tag{30}$$

from which the impedance $Z(\omega) = V_0/I_0$ is derived.

$$Z\,(\omega) = \frac{V_0}{I_0} = R \frac{1}{1 + iQ\frac{\omega^2 - \omega_r^2}{\omega\omega_r}} . \tag{31}$$

$Z(\omega)$ is complex because in general V_0 is not in phase with the excitation I_0. Equation (31) may be re-written to yield the real and imaginary parts of the impedance of a resonator

$$Z(\omega) = Z_r(\omega) + iZ_i(\omega) = R \frac{1 - iQ\frac{\omega^2 - \omega_r^2}{\omega\omega_r}}{1 + \left(Q\frac{\omega^2 - \omega_r^2}{\omega\omega_r}\right)^2} \tag{32}$$

which are shown in Fig. 12.

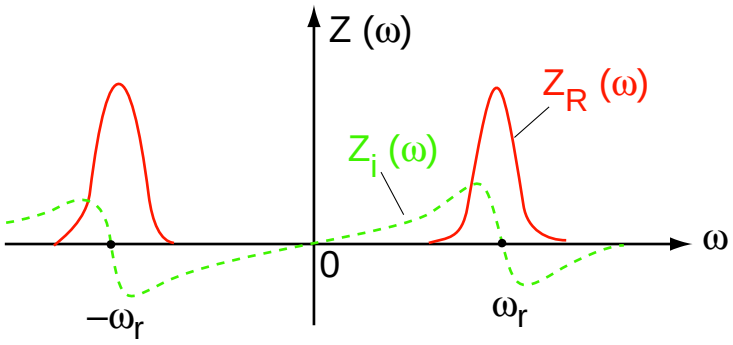

Fig. 12: Real (Z_R) and imaginary (Z_i) parts of the impedance Z of a resonator as a function of ω. Notice that Z_R is an even function of ω whereas Z_i is an odd function of ω.

The expression for the impedance of a narrow-band resonator ('high-Q' cavity) can be simplified near the resonance frequency ω_r (with $\Delta\omega = \omega - \omega_r$) to

$$Z(\omega) \approx R_s \frac{1 - i2Q\frac{\Delta\omega}{\omega_r}}{1 + \left(2Q\frac{\Delta\omega}{\omega_r}\right)^2} . \tag{33}$$

A narrow-band impedance like this one features a high quality factor Q and thus a low damping rate α: once the beam has induced a signal into this object, it will oscillate during many machine turns, memorizing the fields induced during many passages of all bunches (*multi-bunch effects)*. The converse is true for a broad-band cavity: Q is low, the damping rate is large, the induced fields collapse rapidly and are not memorized long enough to have repercussions on subsequent bunches, but only on the bunch itself (*single-bunch effects).*

5. ONE BUNCH AND A NARROW-BAND CAVITY: 'ROBINSON' INSTABILITY

Turning now to bunched beams, the most simple case is the dynamics of one bunch in a narrow-band cavity (historically, this instability was generated by the accelerating cavities). Imagine a bunch performing coherent synchrotron oscillations with the synchrotron frequency ω_s: the bunch rotates in the longitudinal (ΔE–ϕ) phase plane. Projecting this motion on the ϕ-axis, a synchronous detector sees the charge density oscillating around the synchronous phase (see Fig. 13).

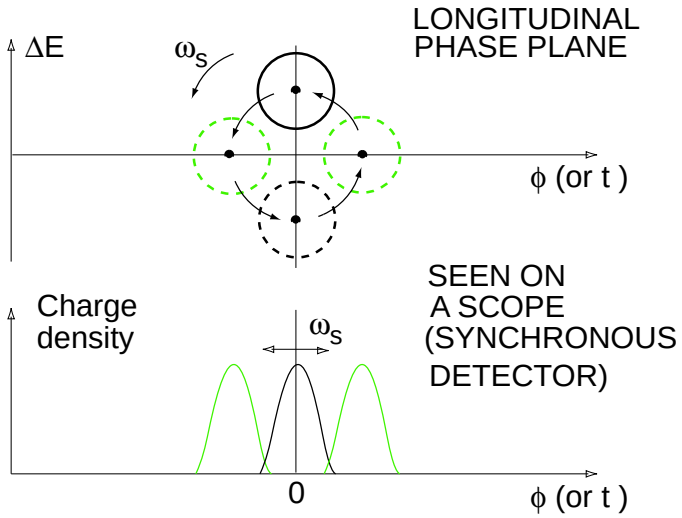

Fig. 13: A bunch performing coherent synchrotron oscillations in the phase plane and as seen by a synchronous phase detector

The energy and phase of the bunch vary periodically with ω_s: in instability jargon, this is called 'rigid bunch' or 'dipole' mode.

Assume that the cavity is tuned at ω_r which is near to, but not exactly at, a multiple n of the bunch's revolution angular frequency $\omega_0 (\omega_r \approx \omega = n\omega_0)$. A close look at Fig. 14 reveals the behaviour of the beam under various conditions:

- For $\gamma < \gamma_t$ and *beam frequency* ω *below resonance frequency* ω_r: whenever $\Delta E > 0$ during the phase oscillation, ω increases (because below transition), sees a larger real impedance R_+ which takes *more* energy from the beam than at R_0, a process which *stabilizes* the dipole oscillation. Conversely,
- for $\gamma < \gamma_t$ and $\omega > \omega_r$ the beam is *unstable.*
- For $\gamma > \gamma_t$ and $\omega < \omega_r$: whenever $\Delta E > 0$ during the phase oscillation, ω decreases (because above transition), sees a lower real impedance R_- which absorbs *less* energy from the beam than at R_0, thus rendering the motion unstable. Conversely,
- for $\gamma > \gamma_t$ and $\omega > \omega_r$ the beam is *stable.*

The instability is removed by fine-tuning of the cavity's resonance frequency ω_r slightly away from the beam frequency $\omega = n\omega_0$. However, nowadays, with the ever increasing performance requirements, an active feedback on the cavity tune proves more efficient for removing this instability.

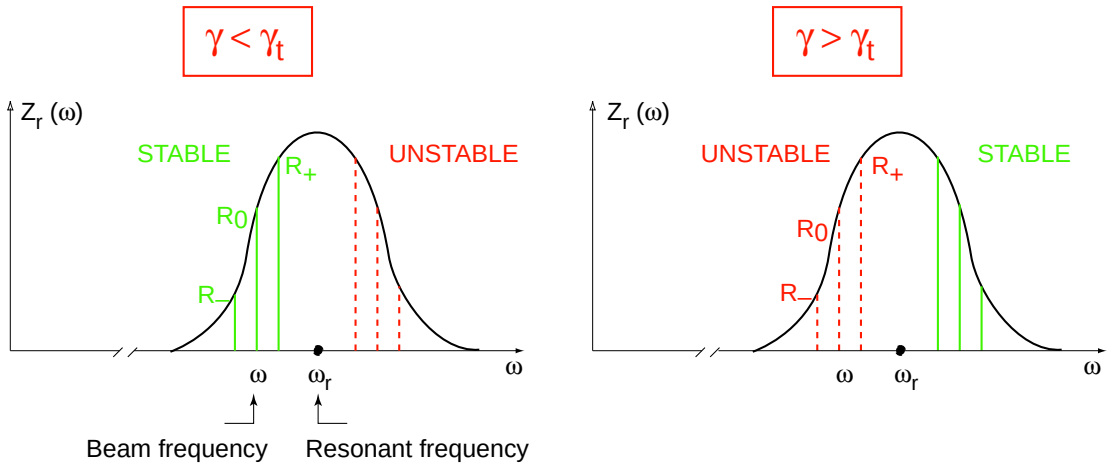

Fig. 14: Stability of a dipole mode bunch oscillation with a narrow-band cavity tuned near a multiple of the bunch revolution frequency, for various cases: below or above transition energy, beam frequency ω below or above the cavity's resonance frequency ω_r.

6. INSTABILITIES WITH MANY BUNCHES

6.1. Coupled-bunch modes and their origin

Modern synchrotrons often work with many bunches (e.g. large colliders and their injectors, beauty factories, synchrotron radiation sources, etc.). Moreover, high-Q cavities, sometimes superconducting, are employed to ensure efficient acceleration. Often these cavities have (undesirable) higher-order modes where the impedance at certain multiples of the revolution frequency takes on high values. As outlined in Section 4, a combination of many bunches and narrow-band resonant impedances enables the latter to memorize the fields for many bunch passages: the induced field due to the first bunch drives the motion of the second bunch, which in turn excites the third bunch, and so on until the first bunch appears back at the cavity for a second time, eventually leading to *coupled-bunch* instabilities. Taking as an example a machine with M = 4 bunches performing synchrotron oscillations, all four bunches may oscillate in phase. However, in addition to this in-phase oscillation mode (mode number n = 0), three other 'modes' of coupling are possible with synchrotron oscillation phase shifts between consecutive bunches of π /2, π, 3π/2 (n = 1, 2, 3). These four modes are depicted in Fig. 15 which shows the motion of the four bunches in the longitudinal phase plane for the four modes.

For a machine with M bunches, there are M modes, with bunch-to-bunch phase shifts $2\pi n/M$, $0 \leq n \leq M - 1$. All these modes are possible, but may grow unstable only in the presence of a high impedance at the mode's frequency.

6.2. Stability of coupled-bunch mode: qualitative analysis

Staying with the example discussed above, there are four bunches in a machine, and a (perturbing) resonator tuned at the revolution frequency. Under what conditions do the bunches become unstable? Three different cases are discussed below, all of them *above transition* energy where particles move *clockwise* in the longitudinal (ΔE, ϕ) plane.

Case 1: the four bunches do not perform coherent synchrotron oscillations. Figure 16 shows the voltage induced into the resonator by each of the four bunches during one machine revolution time T_0, and the motion of each bunch in the longitudinal phase plane – there is no motion in this case as there are no coherent synchrotron oscillations.

The voltage induced by bunch 2 cancels with the one induced by bunch 4, and likewise the voltages generated by bunches 1 and 3 cancel. Hence there is no net induced voltage, the beam is *stable*.

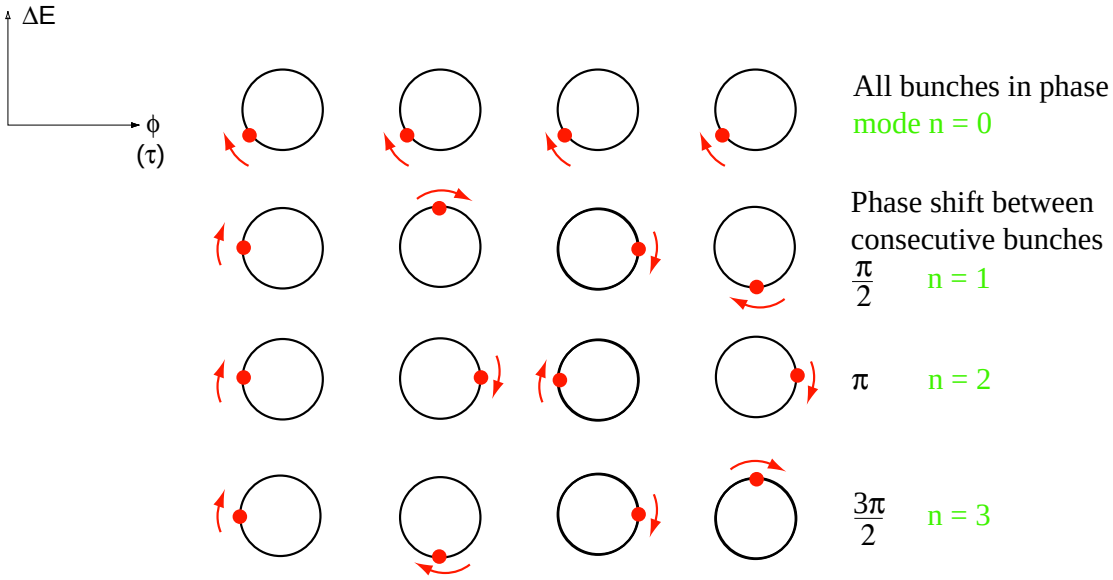

Fig. 15: The four modes of coupled bunch oscillations for a synchrotron with four bunches.

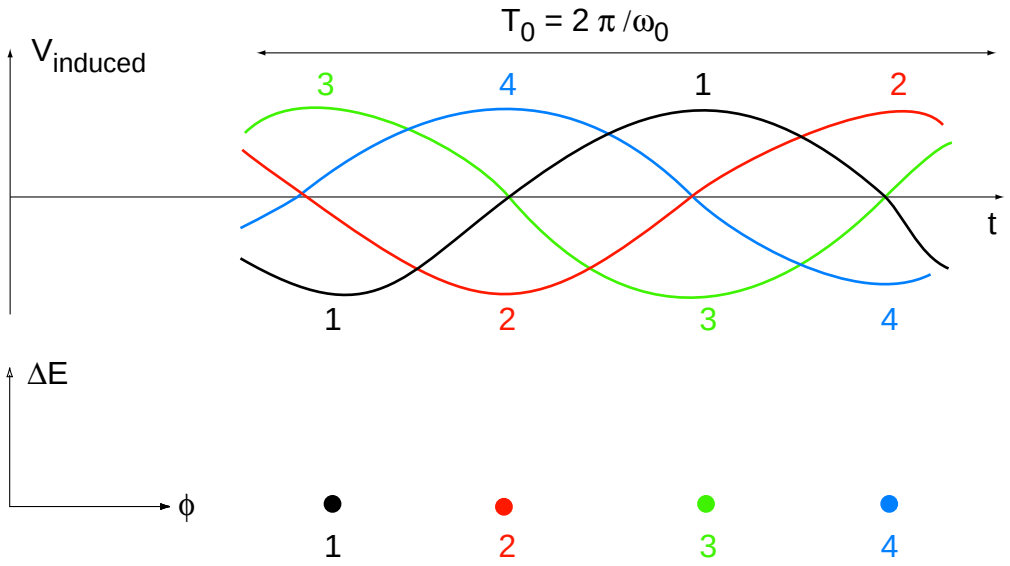

Fig. 16: Voltages induced by each of four bunches in a cavity tuned at the revolution frequency. Bunches do not perform synchrotron oscillations in this case.

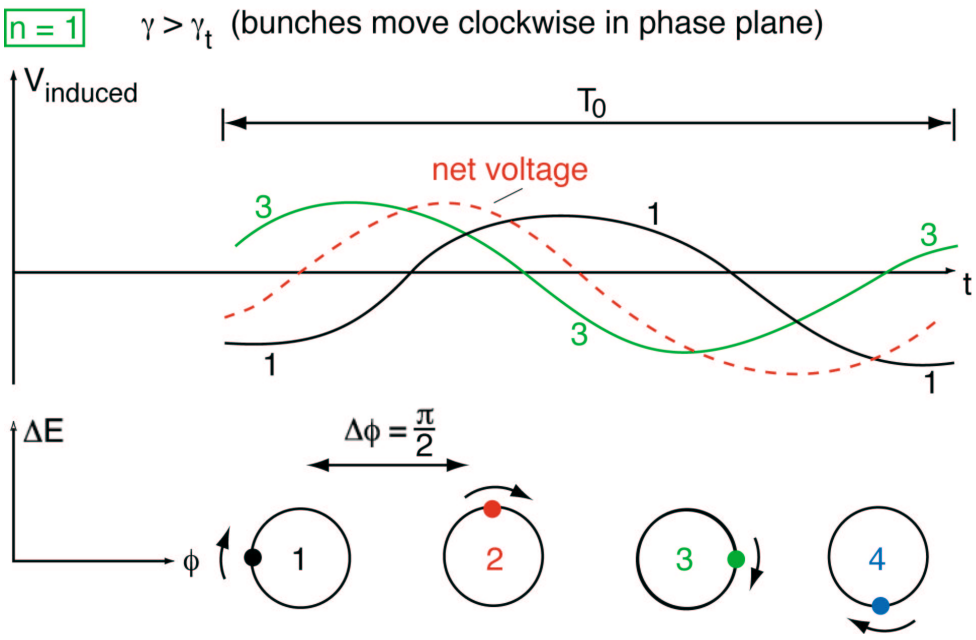

Fig. 17: Voltages induced by two out of four bunches performing coupled synchrotron oscillations with a bunch-to-bunch phase shift of $\pi/2$ (mode n = 1)

Case 2: the four bunches do perform synchrotron oscillation with a bunch-to-bunch phase shift of $\pi/2$ (mode n = 1). Figure 17 explains what happens to these bunches.

While the voltage of bunches 2 and 4 cancel as in Fig. 16, bunches 1 and 3 induce a net voltage. This voltage in turn affects bunch 2 which gets accelerated while bunch 4 is decelerated, thus increasing their synchrotron oscillation amplitude, and the bunches are *unstable*. It is easy to figure out that one-quarter of a synchrotron oscillation later (usually many machine turns), bunches 2 and 4 will drive 1 and 3 unstable.

Case 3: The four bunches perform synchrotron oscillations with bunch-to-bunch phase shift of $3\pi/2$ (mode n = 3) (Fig. 18).

Here again, the voltages induced by bunches 2 and 4 cancel, whereas 3 and 1 induce a net voltage. Bunch 2 is accelerated by this voltage, and bunch 4 decelerated, exactly as for mode n = 1 (Fig. 17). However, the synchrotron oscillation amplitudes of bunches 2 and 4 are both shrinking, so in this case the mode n = 3 is *stable!* Notice that a fixed observer, looking at the oscillating bunches with a synchronous detector, cannot tell the difference between modes n = 1 and n = 3. Yet, one of them is unstable, the other is stable.

In this qualitative approach, modes n = 0 (all bunches oscillating in phase) as well as n = 2 (phase shift π between adjacent bunches) are both stable. The cases discussed above apply above transition energy; below transition, bunches rotate anti-clockwise in the (ΔE–ϕ) plane, thus mode n = 1 becomes stable, and n = 3 unstable.

6.3. Higher-order coupled-bunch modes

So far the most important type of longitudinal oscillation mode, the dipole mode where the bunches rigidly rotate in the phase plane, has been discussed. Under certain conditions, bunches may change their shape, rather than their position, periodically, and this coherent motion may be driven by an impedance and become unstable as well. Defining a further mode number for the bunch shape, m, with m = 1 for the dipole mode, one often observes m = 2 (quadrupole mode), m = 3 (sextupole mode), and sometimes even m = 4 (octupole mode). What do these modes look like?

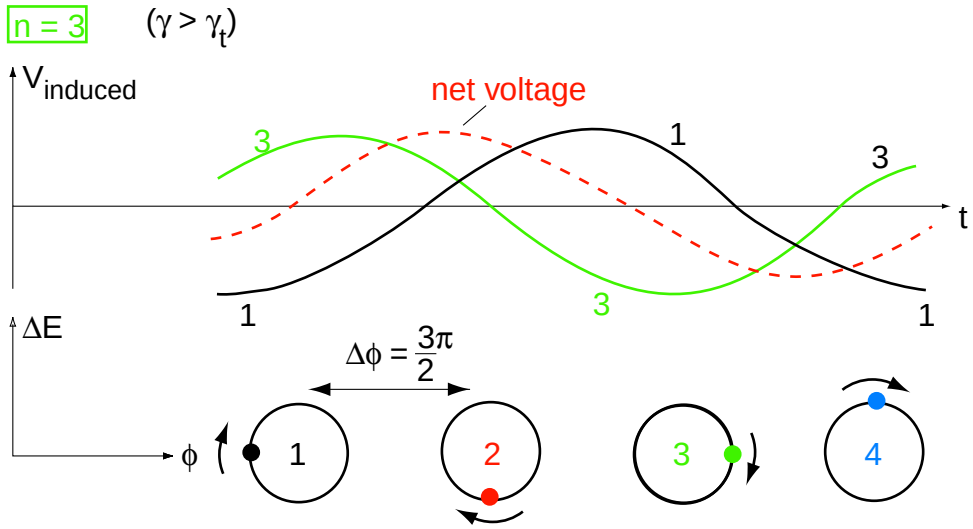

Fig. 18: Voltages induced by two out of four bunches performing coupled synchrotron oscillations with bunch-to-bunch phase shift of $3\pi/2$ (mode $n = 3$)

Various oscilloscope signals as well as the bunch's shapes in the longitudinal phase plane are compiled in Fig. 19 for a machine with five proton bunches (CERN PS Booster). Two adjacent bunches are shown.

What can one learn from Fig. 19?

- A 'mountain range' display is a record of the bunch shape over many turns, where, for example, each tenth turn is visualized and vertically displaced.
- The mountain range displays in Fig. 19a feature a *shift* in the oscillation phase between the two consecutive bunches.
- The higher the mode, the more often the pattern repeats in vertical direction. While the dipole mode is visualized during about one oscillation period, the higher-order modes feature several periods. In fact, while the dipole mode oscillates with the angular synchrotron frequency ω_s ($\sim$ 2π 2 kHz in this case), the higher modes oscillate with $m\omega_s$. This can readily be understood by inspecting the sketches in Fig. 19c (longitudinal phase plane) where the patterns rotate with the synchrotron frequency.

Notice that 'quadrupole' oscillations in the (ΔE–ϕ) plane are often observed after injecting a beam from a lower energy synchrotron. This is due to insufficient adaptation between the respective RF voltages and is called 'longitudinal mismatch'. However, these oscillation do not necessarily give rise to an instability.

7. LONGITUDINAL MICROWAVE INSTABILITY

This instability is observed in synchrotrons with high-intensity bunches. It does not matter whether there are many bunches or just a few, because it is a *single-bunch* effect.

7.1. Signature

High-frequency density modulations along the bunch are observed, as sketched in Fig. 20. The frequency typically ranges from several 100 MHz to several GHz, thus their wavelength is much shorter than the bunch length. The coherent signal is difficult to observe (in general with spectrum analysers), because it becomes rapidly blurred and leads to a very fast and uncontrolled blow-up of the bunch area which may then largely exceed the acceptance of the RF system.

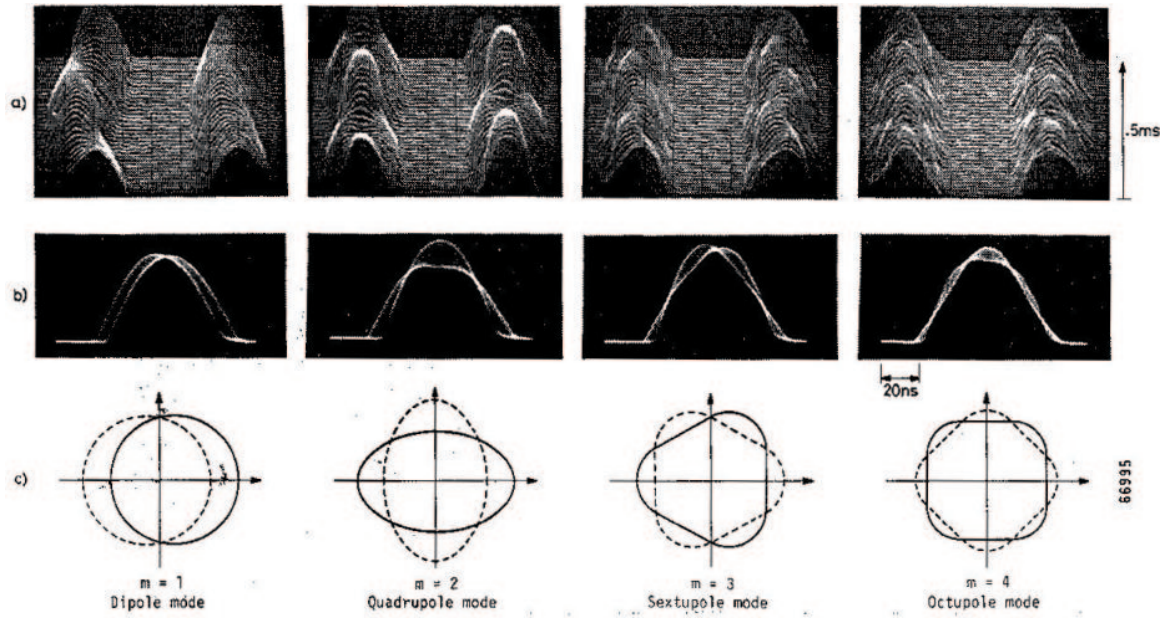

Fig. 19: Dipole and higher-order coupled-bunch oscillation modes as observed for a proton synchrotron with five bunches (CERN PS Booster). The first row (a) shows 'mountain range' displays of two adjacent oscillating bunches, the second row (b) the superimposed signals as observed by a synchronous phase detector, and the third row (c) sketches the bunch shape in the phase plane. The first column covers the m = 1 (dipole) mode, followed by m = 2 (quadrupole), m = 3 (sextupole), m = 4 (octupole) modes.

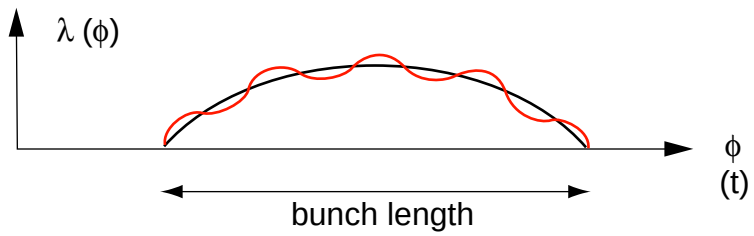

Fig. 20: Signature of longitudinal microwave instability: a high-frequency density modulation is superimposed on the bunch shape $\lambda(\phi)$

Typically, the e-folding time of the growth is shorter than a synchrotron oscillation period. Even lepton machines which normally are less prone to instabilities because of the damping due to synchrotron radiation suffer from this effect because the growth rate is faster than the damping rate. For lepton machines it is also called '*turbulent bunch lengthening*' simply because for a given RF voltage, the blow-up in bunch area manifests itself in a longer bunch.

7.2. The broad-band impedance

In order to drive a density modulation of, for example, 1 GHz unstable, there must be an impedance at $\sim$ 1 GHz. As highlighted in Section 2, the vacuum chambers of synchrotrons, and in particular of older machines which were not built for high intensities in the first place, feature many abrupt cross-section changes, cavity-like elements, etc. All these elements of a synchrotron, together with objects like septum magnets and beam observation devices, may be lumped into one *low-Q 'resonator'*, also called *broad-band impedance.* Recalling the impedance of a resonator (Eq. 33), one calculates this broad-band impedance

$$Z(\omega) = R_s \frac{1 - iQ\frac{\omega^2-\omega_r^2}{\omega\omega_r}}{1 + \left(Q\frac{\omega^2-\omega_r^2}{\omega\omega_r}\right)^2} \tag{34}$$

with $Q \approx 1$ and the resonance frequency $\omega_r \approx 1$ GHz. This impedance $Z(\omega)$ is sketched in Fig. 21.

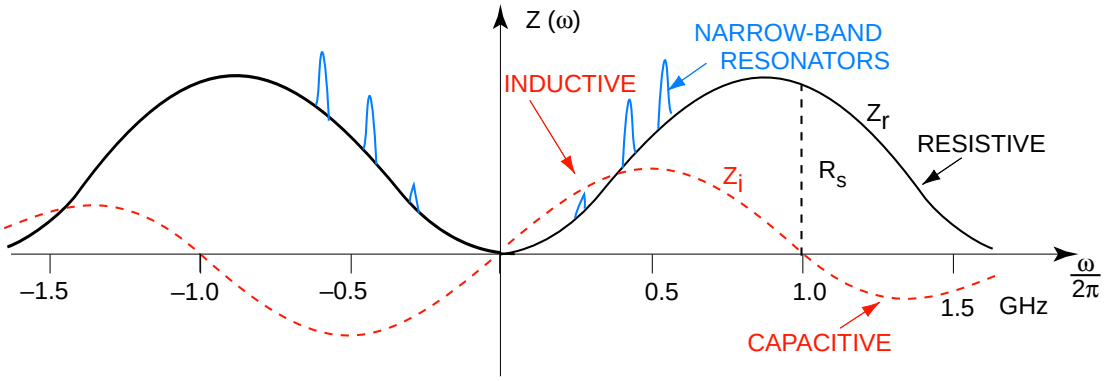

Fig. 21: Broad-band impedance with resonance frequency about 1 GHz and $Q \approx 1$. This impedance approximates the sum of individual impedances of most elements of a synchrotron.

In contrast with a narrow-band impedance, a wide-band impedance has a very short 'memory' for fields induced by a bunch, thus there is barely any coupling between adjacent bunches. Therefore, this is a single-bunch effect where the head of the bunch induces a high-frequency field which increases along the bunch. Obviously this model, using the approximate broad-band impedance, lacks precision, but has the merit of explaining the observed effect rather well.

In order to estimate this impedance, one measures its value for small ω, where according to Eq. (34) $Z(\omega)$ may be approximated by

$$Z(\omega) \approx i\frac{R_s\omega}{Q\omega_r} = i\frac{R_s}{Q}\,\frac{\omega}{\omega_0}\,\frac{\omega_0}{\omega_r}\,. \tag{35}$$

Replacing the ratio ω/ω_0 by n, and with $Q = R_S/(\omega_r L)$ (Eq. 28) one finds for the low-frequency impedance

$$\left|\frac{Z}{n}\right|_0 = L\omega_0\,. \tag{36}$$

This is an inductive impedance, normalized to n, the multiple of the revolution frequency ω_0. While $|Z/n|$ is constant for small ω, $|Z|$ rises linearly with ω as shown in Fig. 21 (dotted line).

The value of $|Z/n|$ determined in this way is conveniently called the *impedance of the synchrotron* and is given in Ω. For older machines, this value is in the ballpark of 20–50 Ω whereas for more modern machines, often designed on purpose to minimize this figure, it is of the order of 1 Ω.

7.3. Stability limit

As for the coasting beam instability, experience has shown that, also in this case, a stability criterion provides a rule of thumb to decide whether or not a bunch will suffer from microwave instabilities. One applies the Keil–Schnell coasting beam criterion (26) to the *instantaneous* current and momentum spread in the bunch

$$\left|\frac{Z}{n}\right| \leq F\,\frac{m_0c^2\beta^2\gamma\,|\eta|}{e}\,\left[\frac{(\Delta p/p)^2}{I}\right]_{\text{instant.}} \tag{37}$$

where $\Delta p/p$ and I are the instantaneous relative momentum spread and beam current, respectively, and F a form factor of the order of unity for protons, and about 8 for leptons ('Keil–Schnell–Boussard' criterion).

It is interesting to note that a bunch with a given longitudinal emittance and given bunch population features a largely different stability behaviour depending on its shape in the phase plane: as sketched in Fig. 22, short bunches with large $\Delta p/p$ are more stable than long bunches with low $\Delta p/p$.

This may be explained by inspecting relation (37) where the ratio $(\Delta p/p)^2/I$ is larger in the short bunch case, thus allowing for a larger limit impedance $|Z/n|$ or a larger current I.

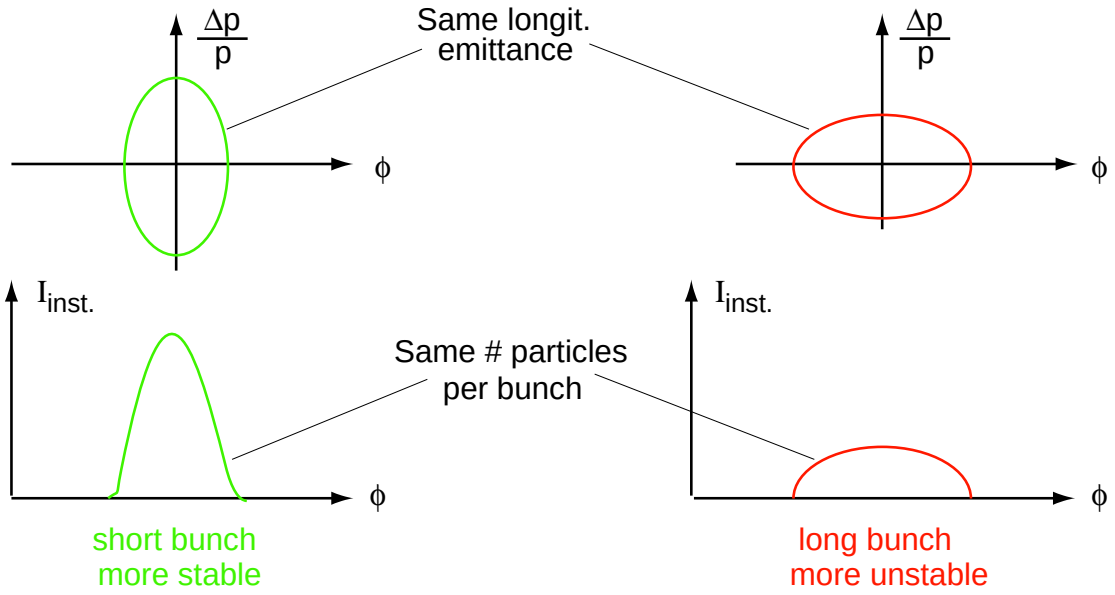

Fig. 22: Bunch shape in the phase plane and microwave instability: short bunches with large momentum spread are more stable than long bunches with small momentum spread

8. FURTHER READING

This paper is a write-up of a one-hour CAS Lecture. It is very much inspired by the lecture notes 'Instabilities' by E.J.N. Wilson, edited in 1997. There are quite a few other lecture notes which may guide the reader towards further insight in the subject:

- A. Hofmann's classical 1976 write-up of his lecture on longitudinal phenomena in the first CAS [1].
- J.L. Laclare's very complete analysis on both coasting and bunched beam instabilities (transverse and longitudinal) [2], [3].
- A more pragmatic description of instabilities which includes their observation and correction by J. Gareyte [4].
- A special treatise on multi-bunch instabilities and their cure by F. Pedersen [5].
- Rather recent lecture notes on instabilities and beam intensity limitations in synchrotrons, with special emphasis on the findings in lepton machines, by S. Myers [6].
- Of course, A.W. Chao's book, which covers all collective beam instabilities, will enlighten any interested reader [7].

References

[1] A. Hofmann, Single beam collective phenomena – longitudinal, 1976 CAS Erice, CERN 77–13, p. 139.

[2] J.L. Laclare, Coasting beam instabilities, 1992 CAS Jyväskylä, CERN 94–01, p. 349.

[3] J.L. Laclare, Bunched beam coherent instabilities, 1985 CAS Oxford, CERN 87–03, p. 264.

[4] J. Gareyte, Observation and correction of instabilities in circular accelerators, CERN SL/91–09 (AP), Joint US-CERN School, Hilton Head Island, USA, 1990.

[5] F. Pedersen, Multi-bunch instabilities, CERN PS/93–36(RF), Joint US-CERN School, Benaldamena, Spain, 1992.

[6] S. Myers, Instabilities and beam intensity limitations in circular accelerators, CERN-SL/97–48(DI), CAS Course on Synchrotron Radiation, Grenoble, 1996.

[7] A.W. Chao, Physics of collective beam instabilities in high-energy accelerators, John Wiley&Sons, New York, 1993.